Numerical Solutions of Laminar Separated Flows

PATRICK J. ROACHE*

AND

THOMAS J. MUELLER†

University of Notre Dame, Notre Dame, Ind.

Numerical techniques and solutions for both incompressible and compressible laminar separated flows using time-dependent finite difference equations are presented. These include backstep flows with and without splitter plates, and flow over square cavities. Conservative forms are used, and the Transportive Property is defined and briefly discussed. Upwind differencing is used for the advection terms. Particular attention is paid to the boundary-condition problems, especially the adjusting upstream vorticity, the vorticity at the sharp corner and the downstream continuation in incompressible flow, and the adjusting inflow through the top of the mesh and the wall density in supersonic flow. Computational stability was maintained throughout the wide range of parameters investigated. The phenomenon of backstep separation off the base below the sharp corner, which was first found experimentally by Hama in supersonic flow, is demonstrated in both incompressible and compressible flow. The separation point moves down from the conjectured limit position at the sharp corner toward a Stokes flow limit as the Reynolds number is decreased.

Nomenclature

C = Courant number $= c\Delta t/\Delta x$
C_p = pressure coefficient: $(P - P_0)/q_0$
c = isentropic speed of sound
DSL = dividing streamline
E = Eckert number
E_s = ρe_s
e = specific internal energy
e_s = stagnation value of e: $e_s = e + V^2/2$
h = backstep height or cavity depth
L = characteristic length, taken as $L = h$
M = Mach number
Nu = Nusselt number
n = distance normal to wall
P = pressure
Pr = Prandtl number
q = dimensionless dynamic pressure: $q = \frac{1}{2}(u^2 + v^2)$
R = Reynolds number
T = temperature
t = time
u,v = x, y components of velocity
V = total velocity
x, y = Cartesian coordinates
β = mesh aspect ratio: $\beta = \Delta x/\Delta y$
γ = ratio of specific heats
Δ = finite difference
δ = boundary-layer thickness
$\delta/\delta x$, etc. = finite difference form $\partial/\partial x$, etc.
Λ = Pohlhausen pressure gradient parameter
μ = coefficient of viscosity
ξ = vorticity: $\xi = +\nabla \times \mathbf{V}$
ρ = density
Σ = summation
ψ = stream function
∇ = del operator

Subscripts

A = value at upstream side of sharp corner
B = value at downstream side of sharp corner; also, value in the base region
crit = critical
$\mathfrak{C}$ = centerline
e = value at edge of inflow boundary layer
f = regular field node point
i = a node point $\frac{1}{2}$ cell width inside the body
i,j = node indexes in x, y directions
ic,jc = i, j values at the sharp corner
iL,jL = largest i, j values in the computing mesh
0 = inflow freestream conditions
R = value at reattachment
s = stagnation (reservoir) value
T = total (reservoir) value
w = value at a wall

Superscripts

n = time level
$(\bar{\ })$ = dimensional quantity
$(\hat{\ })$ = average quantity

Presented as Paper 68-741 at the AIAA Fluid and Plasma Dynamics Conference, Los Angeles, June 24–26, 1968; submitted August 8, 1968; revision received September 10, 1969. This research was partially supported by the Atomic Energy Commission and partially by NASA under Grant NXG (T)-65, and was part of the PhD dissertation of the first author.

* Graduate Student, Aero-Space Engineering Department; presently Staff Member, Technical, Numerical Fluid Dynamics Division, Aerothermodynamics Research Department. Member AIAA.

† Professor, Department of Aero-Space and Mechanical Engineering. Associate Fellow AIAA.

I. Introduction

ALTHOUGH separated flows have been of great interest during the past two decades, completely adequate analytical solutions have not been possible because of the complex nature of these flows. Analytical predictions of important gross effects such as base pressure and drag, etc., based on a flow model approach, have been successful. However, these semiempirical analyses have proceeded without benefit of a good understanding of the entire separated flow region and therefore cannot be applied with confidence to situations where the results are not known a priori from experiments.

The investigation described herein was undertaken to increase understanding of the structure and phenomena of laminar separated flows. In this paper are presented the necessarily brief descriptions of the finite difference methods used and the numerical solutions obtained for planar laminar separated flows, both incompressible and compressible. They are taken from Ref. 1, which contains further details of the results; descriptions of numerical experiments with other

boundary conditions and with other basic differencing schemes; reviews of experiments, theories, other numerical methods, and other numerical studies of separated flows; and some discussion of the problems of existence, uniqueness, stability, and convergence.

II. Basic Numerical Methods for Incompressible Flow

The basic incompressible-flow equations used are the vorticity transport equation in conservation form,

$$\partial\xi/\partial t = -\nabla\cdot(\mathbf{V}\xi) + (1/R_0)\nabla^2\xi \tag{1}$$

and the Poisson equation for stream function,

$$\nabla^2\psi = -\xi \tag{2}$$

where

$$\partial\psi/\partial y = u,\ \partial\psi/\partial x = -v \tag{3}$$

$$\xi = \nabla\times\mathbf{V} = -\partial u/\partial y + \partial v/\partial x \tag{4}$$

In these equations distance has been normalized by the characteristic length, L, time by the advective time constant $(L/\bar{u}_0)$, and vorticity by $(\bar{u}_0/L)$. Although the term $\nabla\cdot(\mathbf{V}\xi)$ could be reduced to $\mathbf{V}\cdot\nabla\xi$ by the use of the incompressible continuity equation $\nabla\cdot\mathbf{V} = 0$, we leave Eq. (1) in its unexpanded form. Proper finite differencing of this conservation form[2] then gives a conservative system, i.e., the Gauss divergence theorem is identically satisfied by the finite difference forms, regardless of the accuracy of the solution.

The parabolic equation (1) is solved by explicit marching in time from some initial condition, the steady-state solution being attained (if it exists) as an asymptotic time solution.‡ At each time step, the elliptic Eq. (2) is solved iteratively by optimum overrelaxation. In Ref. 1, it is shown that numerical instabilities of explicit finite difference methods can be simply related to the familiar concepts of static and dynamic instabilities. Dynamic instabilities are caused by too large a time step. Static instabilities result from the form of the finite difference equation, and lead to limitations of the maximum Reynolds number based on the finite difference cell size.

The basic method used for Eq. (1) at interior field points is as follows: the velocity components are obtained from the stream function distribution by centered differencing of Eq. (3);

$$u_{ij} = \frac{\psi_{i,j+1} - \psi_{i,j-1}}{2\Delta y},\ v_{ij} = -\frac{\psi_{i+1,j} - \psi_{i-1,j}}{2\Delta x} \tag{5}$$

the vorticity is then advanced in time;

$$\xi_{ij}{}^{n+1} = \xi_{ij}{}^{n} + \Delta t\left[-\frac{\delta(u\xi)^n}{\delta x_{ij}} - \frac{\delta(v\xi)^n}{\delta y_{ij}} + \frac{1}{R_0}\frac{\delta^2\xi^n}{\delta x_{ij}{}^2} + \frac{1}{R_0}\frac{\delta^2\xi^n}{\delta y_{ij}{}^2}\right] \tag{6}$$

and the diffusion terms are represented by the usual centered difference form, as in

$$\delta^2\xi/\delta x_{ij}{}^2 = \xi_{i+1,j}{}^n + \xi_{i-1,j}{}^n - 2\xi_{ij}{}^n/\Delta x^2 \tag{7}$$

The advection terms are represented by the method of upwind differencing, which has appeared in the literatures under various labels and with different rationales. Meteorologists have long known of the stabilizing effect of "upwind"[3,4] or "weather"[6] differencing.§ Mathematicians analyze the difference equations with positive coefficients.[4,6] Many authors[7–9] credit Lelevier via Richtmeyer,[9] and others[10,11] credit the paper of Courant, Isaacson, and Rees[12] (in which they demonstrate the essential link of the method to the theory of characteristics) and use the term "upstream differencing."[11] Longley's "Type II" scheme,[13] Filler and Ludloff's first method,[14] the "donor cell mass differencing" of Gentry, Martin, and Daley,[15] and the method of Thoman and Szewczyk[16] are all reapplications of the method, without historical reference.

The upwind difference form of the advection terms is as follows:

$$\frac{\delta(u\xi)^n}{\delta x_{ij}} = \begin{cases}(u\xi)_{i+1,j}{}^n - (u\xi)_i{}^n/\Delta x \text{ for } u < 0\\ (u\xi)_{i,j}{}^n - (u\xi)_{i-1,j}{}^n/\Delta x \text{ for } u > 0\end{cases} \tag{8}$$

Similar evaluations are used for $\delta(v\xi)^n/\delta y_{ij}$. In this first-order method, information is advected into a cell only from those cells that are upwind of it.¶ Conversely, information is advected from a cell only into those cells which are downstream of it. This is, of course, physically correct, and leads to the following definition[1] of the Transportive Property. A finite difference formulation of a flow equation possesses the Transportive Property if the effect of a perturbation in a transport property is advected only in the direction of the velocity.

Only upwind differencing methods can possess this property. In any method using space centered differences for the advection terms, the effect of a perturbation is advected upstream, against the velocity.[1] A finite difference method which possesses the Transportive Property maintains the integral kinematic property of the continuum solution, in the same way that one which possesses the Conservative Property maintains the integral Gauss divergence property of the continuum solution.

The physical relevance of upwind differencing has also been suggested or implied by the descriptions of Frankel[5] in referring to the "unidirectional flow of information," of Gentry, Martin, and Daley,[15] who used "donor cell mass differencing", and by Thoman and Szewczyk[16] who "employ the average vorticity of the cells from which the vorticity is transported."

The critical time step to avoid dynamic instability is given by

$$\Delta t_{\text{crit}} = \frac{1}{u_{ij}/\Delta x + v_{ij}/\Delta y + (2R_0)(1/\Delta x^2 + 1/\Delta y^2)} \tag{9}$$

The Δt used was from 0.8 to 0.95 of Δt_{crit}.

The stability of this method, along with the boundary conditions to be discussed in Sec. III, has been demonstrated by calculations for R_0 from 0.1 to 100,000. However, the accuracy of the method in resolving viscous effects deteriorates at high R_0, because the method implicitly introduces an effect which resembles an artificial viscosity effect.[1] It can be shown that in regions where the Prandtl boundary-layer approximations[17] are valid, this artificial viscosity effect is negligible. (This helps explain the surprising agreement of the numerical calculations of Ref. 16 with experiment.) But for more general flow situations, only qualitative accuracy can be claimed at high R_0.

Once the new ξ distribution at $(n+1)$ is known from Eq. (6), the new ψ distribution is found from (2) by iteration, using overrelaxation.

The criteria used to determine convergence for the solution of ψ at each time step and for the asymptotic steady-state solution of ξ were very demanding. For example, $\Sigma_{ij}|\psi_{ij}|$ did not change at all, to all 8 significant figures printed out, for as many as 50 time steps. Thus, convergence was un-

‡ This philosophy and approach to the problem have been well known for years. Frankel[5] perceptively discussed the interpretation of time-step equations as iterative relaxations of the steady-state equations as early as 1950.

§ The opposite of weather differencing is lee differencing,[5] which is unconditionally unstable.

¶ When u reverses sign near a node point, a modification to the basic upwind difference scheme (8) is required in order for strict conservation to hold.[7]

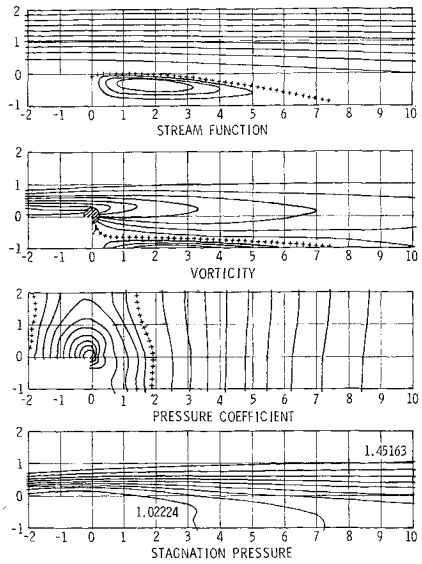

Fig. 1 Incompressible flow over a backstep with R_O = 100. δ/h = 1, Λ = 0, no-slip center-line. $\Delta\psi$ = 0.17000 above +, $\Delta\psi$ = 0.00737 below +, ψ = 0 at +. $\Delta\xi$ = 0.21987 above +, $\Delta\xi$ = 0.11783 below +, ξ = 0 at +. ΔC_p = 0.01879 at +, ΔC_p = 0.00629 below +, C_p = 0 at +. ΔP_T = 0.05367.

equivocally reached, to the single-precision accuracy of the computer.

After the ξ and ψ solutions were reached, the temperature distribution was determined from the energy equation, including a dissipation term (nonzero Eckert number) using methods analogous to those used on the vorticity transport equation. The pressure is determined from a Poisson equation, analogous to Eq. (2).

III. Numerical Boundary Conditions for Incompressible Flow

A major part of the present work involved the development of realistic, accurate, and stable boundary conditions. The surfaces referred to in the following discussion are shown in Fig. 1. In this mesh system, node points lie on the walls.

No-slip walls appear at the upstream wall, at the base, and along the centerline when a wind-tunnel "splitter plate" is used. Along these surfaces, $\psi = 0$, following convention. The vorticity is determined in the customary manner, by expanding ψ out from the walls in a Taylor series and invoking the no-slip condition. The result is

$$\xi_w = -2(\psi_{w+1} - \psi_w)/\Delta n^2 \tag{10}$$

where w refers to a wall point, and Δn is the distance normal to the wall, from (w) to $(w + 1)$.

When the centerline is not a splitter plate, the backstep geometry of Fig. 1 represents the symmetrical half of the base flow problem (valid only for the subcritical wake). Symmetry then requires

$$\xi_{\mathbb{Q}} = 0 \tag{11}$$

The upstream inflow boundary is partly determined by specifying a boundary-layer inflow, and partly develops as part of the solutions. The inflow stream function is set by integration of the fourth-order Pohlhausen boundary-layer solution[17] for u. Thus ψ and $\partial u/\partial y$, one term of ξ, are specified at inflow. The other term of ξ, $\partial v/\partial x$, is determined by approximating $\partial^2 v/\partial x^2 = 0$ at inflow. There is no particular physical justification for this boundary condition. It is simply the least restrictive method found by numerical experimentation which permits convergence.

The boundary-layer equations do not correctly represent the flow at low R_0, and the Pohlhausen solution is only an approximate solution to the boundary-layer equations. At $R_0 = 0.1$, for example, we do not suggest that the input Pohlhausen profile used represents an accurate solution of flat plate flow ahead of the base. It is merely a convenient, one-parameter family of u velocity profiles by which we study the effects of upstream velocity profile shape on the separated flow, and it qualitatively represents a meaningful flow condition.

The boundary condition at the upper boundary or lid was somewhat disappointing. It had been desired to model the backstep with no upper boundary (free-flight case), but numerical experimentation did not disclose a method of allowing inflow through the mesh at the lid without destabilizing the solution. The most nearly free condition found is to use an impermeable slip wall at the lid. The value of ψ is set from the inflow boundary conditions, with $\psi_{\text{lid}} = \psi_{1,jL}$. The vorticity condition has been set by other authors by specifying a constant value of u at the lid,[16,18,19] or by setting $\xi_{\text{lid}} = 0$,[20] which approximately implies $\partial u/\partial y = 0$ at the lid. We use a less restrictive condition,

$$\xi_{i,jL} = \xi_{i,jL-1} \tag{12}$$

where $\xi_{i,jL-1}$ develops as part of the solution. This approximates $\partial^2 u/\partial y^2 = 0$ at the lid. It is almost equivalent to a linear extrapolation of u out to the lid.

The downstream continuation problem was treated for high R_0 flows in a manner following Thoman and Szewczyk.[16] We approximate a zero gradient for ξ and use a linear extrapolation for ψ.

$$\xi_{iL,j} = \xi_{iL-1,j} \tag{13}$$

$$\psi_{iL,j} = 2\psi_{iL-1,j} - \psi_{iL-2,j} \tag{14}$$

The latter condition approximates $\partial v/\partial x = 0$ at outflow.

These are the least restrictive boundary conditions which still maintain computational stability, even when vortex shedding is present. But at low R_0 (10 and less), this vorticity condition was too restrictive, giving an abrupt change in $\partial\xi/\partial x$ near outflow. More realistic results were obtained with a much less restrictive approach. The vorticity at outflow was evaluated from the unsteady vorticity transport equation, as done at interior mesh points. Because of the upwind differencing, there is no further approximation involved in the advection terms. Also $\partial^2\xi/\partial y^2$ is evaluated at iL by regular interior point differencing. The remaining term, $\partial^2\xi/\partial x^2$, is evaluated at one mesh point inside the outflow boundary by setting $(\partial^2\xi/\partial x^2)_{iL,j} = (\partial^2\xi/\partial x^2)_{iL-1,j}$. By itself, this procedure is statically destabilizing. The direction of the restoring displacement has been put out of phase by the shift in node point; it is brought back in phase by another shift, in time level, from (n) to $(n - 1)$. The result is

$$\xi_{iL,j}{}^{n+1} = \xi_{iL,j}{}^{n} + \Delta t\left[-\left.\frac{\delta(u\xi)}{\delta x}\right|_{iL,j}^{n} - \left.\frac{\delta(u\xi)}{\delta y}\right|_{iL,j}^{n} + \frac{1}{R_0}\left.\frac{\delta^2\xi}{\delta x^2}\right|_{iL-1,j}^{n-1} + \frac{1}{R_0}\left.\frac{\delta^2\xi}{\delta y^2}\right|_{iL,j}^{n}\right] \tag{15}$$

The vorticity at the sharp corner (ic,jc) requires special consideration. Seven different methods[1] were tried, five of which were more or less successful. Some involved rounding off the corner, whereas others involved using upstream wall values or otherwise biasing the results toward the usual anticipation of separation occurring at the corner. We wish to model as well as possible the mathematical limit of a sharp corner, and so use discontinuous values of $\xi_{ic,jc}$. ξ_A is evaluated by using the no-slip wall equation (10), considering the corner as part of the upstream wall, and ξ_B by considering it as part of the base. Then ξ_A or ξ_B is used for $\xi_{ic,jc}$, de-

pending on whether it is needed, in an interior point difference equation, either upstream or downstream of the corner.

The boundary conditions for pressure are all von Neumann boundary conditions on the pressure gradient, obtained from the primitive steady-state momentum equations,

$$\partial P/\partial x = -u(\partial u/\partial x) - v(\partial u/\partial y) + (1/R_0)\nabla^2 u \quad (16)$$

and its y counterpart. The right member is determined from the ξ-ψ solution. An obvious approach is to calculate the kth iterate for P at all internal points, and then reset the boundary values in accordance with Eq. (16). At the base, for example,

$$P_{ic,j} = P_{ic+1,j} - \left.\frac{\partial P}{\partial x}\right|_{ic+1/2,j} \Delta x \quad (17)$$

where the pressure gradient is the average of those evaluated at (ic,j) and at $(ic+1,j)$, using Eq. (16). This method does not converge. It drifts, slowly but endlessly. To achieve convergence, Miyakoda[21] has shown that the gradient condition Eq. (16) must be included in the basic interior point differencing for the Poisson pressure equation at node points one cell in from the boundary.[1]

IV. Basic Numerical Methods and Boundary Conditions for Compressible Flow

The numerical methods used for the compressible flow solutions will be only briefly described here. The conservation form of the viscous compressible Navier-Stokes equations were used. The independent flow variables are ρ, ρu, ρv, and $E_s = \rho e_s = \rho(e + v^2/2)$. E_s is the reservoir internal energy per unit volume. An ideal gas is assumed. Some solutions were obtained using constant properties, and others using $\mu \propto T$.

Upwind differencing was again used for the advection terms, as in incompressible flow. The method is more significant to compressible flow, since it maintains the correct characteristic sense of the continuum equations. Other derivatives are approximated by centered differences in space and forward differences in time.

In addition to the Courant-Friedrichs-Lewy[22] restriction that the Courant number $C_0 < 1$, Kurzrock's[8] additional stability restriction was required. Instability still occurred for R_0 much less than 1000. This instability was removed by applying to the viscous terms a two-step, two-time level analog of the one-step, three-time level Du Fort-Frankel method[23] of incompressible flow.[1] The stability of this method, along with the boundary condition to be discussed, has been demonstrated by calculations for R_0 from 10–100,000, and for M_0 from 0.5–6.

The boundary conditions along walls are best accommodated in compressible flow by a mesh system in which the walls lie between node points. Solutions were also obtained with a mesh system in which the node points lie on the walls, but this mesh creates difficulties in evaluating the wall density. The methods commonly used (extrapolation of ρ, evaluations of ρ through pressure gradients and wall temperatures, etc.) are not conservative. Mass disappears from, or is created within, the system. For flat-plate calculations, one can get away with these approximations. But in the case of the backstep, such nonconservative tricks lead to a slow but monotonic divergence of wall density to zero and beyond in the neighborhood of the sharp corner.**

A related difficulty occurs in modeling an adiabatic wall. A would-be adiabatic wall should be adiabatic numerically, i.e., in the sense of maintaining the conservation laws in finite difference form. To accomplish this, one must set $T_i = T_f$ (or, in the first mesh system, $T_w = T_{w+1}$). Elegant polynomial extrapolations to represent $\partial T/\partial n = 0$ at the wall are not valid since if $T_i \neq T_f$, the finite difference calculation at f will give a heat flux out from the wall, and the wall is not *numerically* adiabatic. The general caution is not to treat node-point values merely as one would treat experimental data points. To do so often destroys the essential conservation character of the calculations.

Nothing is assumed about the pressure gradient at a no-slip wall. Rather, the pressure gradient is evaluated by one-sided differences applied at the adjacent interior point.

The inflow boundary conditions are completely fixed by an adiabatic wall boundary-layer solution. (At low R_0, this results in a considerable v component of inflow velocity.) The outflow conditions are treated as in the incompressible vorticity transport equation, with the x pressure gradients evaluated by one-sided differences. The technique of evaluating the diffusion terms for the outflow boundary at one node point inside the mesh, but without the time shift of the present method, has been previously used by Eaton and Zumwalt[24] in their study of blast wave penetration.

The boundary conditions at the lid are treated very successfully for supersonic flow. Inflow and outflow do occur across the lid, the details developing as part of the numerical solution. A simple wave inviscid approximation is used. After each time-step calculation is completed and the new variables have been calculated at one node below the lid, the left-running Mach line which passes through each boundary node is located from elementary gas dynamic relations, using linear interpolation for values between nodes. The simple wave assumption of constant properties along the Mach line then determines all flow variables at the upper node point. The stability of the method is not sensitive to the details of the arithmetic; Allen[25] has successfully used this same approach, with a different calculational procedure and a different basic finite difference method.

V. Numerical Solutions—Incompressible Flow

In this section, the numerical results for incompressible flow will be presented and discussed. The basic mesh configuration used for the backstep problem consisted of a 10×10 cell corner in a 40×30 cell field, with $\beta = \Delta x/\Delta y = 2$. Thus the inflow condition was located two base heights upstream of the corner and the frictionless wind-tunnel wall was two base heights above the corner. The length of the mesh was extended as far as 80 cells to accommodate the longer recirculation region for some conditions. Most runs were made with a no-slip centerline condition, corresponding to a physical splitter plate. Other boundary conditions have been discussed in Section III.

Figure 1 presents the contour plots for the basic case of this investigation. Most of the other runs present variations of one or more of the parameters of this figure and are therefore to be compared with it. The backstep $R_0 = 100$, the inflow boundary-layer thickness $\delta/h = 1$, and the Pohlhausen parameter $\Lambda = 0$, indicating a zero pressure-gradient profile at inflow. The (0,0) origin is located at the sharp corner.

Part A of Fig. 1 is a stream function plot. The dividing streamline ($\psi = 0$) or DSL is marked with a + symbol. The increased spacing between the streamlines at constant $\Delta\psi$ indicates the lower velocity and therefore lower mass flux in the lower portions of the boundary layer. The extrapolated separation point occurs less than one cell below the sharp corner, and reattachment occurs between 7 and 8 base heights downstream of the corner. The DSL appears concave upwards near reattachment. The streamline near $y = 1$ at the inflow slopes slightly upward from $x = -2$ to -1, due to the growth of the boundary layer. Then the streamlines curve downward and proceed over the step.

Part B is a vorticity contour plot. The zero vorticity line is marked with a + symbol. The heavy concentration of contour lines near the sharp corner (shaded area) indicates a high vorticity gradient in this region, as expected. Within

** The authors are indebted to J. S. Allen of Princeton Univ. for his advice that conservation was the key to this problem.

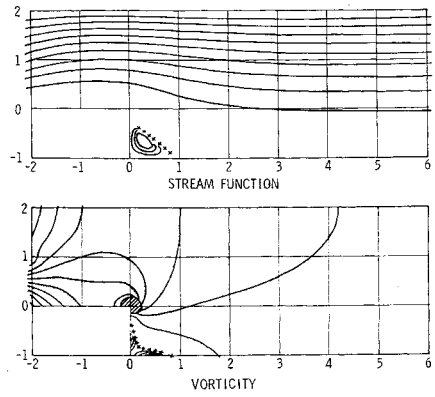

Fig. 2 Incompressible flow over a backstep with R_0 = 0.1. δ/h = 1, Λ = 0, no-slip centerline. $\Delta\psi$ = 0.17000 above +, $\Delta\psi$ = 0.00024 below +, ψ = 0 at +. $\Delta\xi$ = 0.19904 above +, $\Delta\xi$ = 0.01367 below +, ξ = 0 at +.

the upstream boundary layer, the constant vorticity lines generally follow the streamline shapes. This will occur for any transport property when advection terms dominate, or in this case when $R_0 \gg 1$. Outside the boundary layer, no vorticity contour lines appear, indicating a region of nearly constant ($\xi = 0$) vorticity.

Part C is a contour plot of the pressure coefficient $C_p = (P - P_0)/q_0$, where

$$q_0 = \tfrac{1}{2}(u_0^2 + v_0^2)$$

is the dimensionless dynamic pressure at the reference position, taken one node point in from the inflow boundary and one node point down from the lid. C_p is negative approaching the corner and in the base region, indicating positive pressure drag of the backstep due to the viscous pumping effect. Between 1 and 2 base heights downstream, C_p is again positive, in agreement with the simple inviscid, one-dimensional Bernoulli approximation requiring a pressure increase in an expansion. The pressure in the downstream region is nearly one-dimensional, as indicated by the nearly vertical contour lines, implying that $\partial P/\partial y \simeq 0$. Also at the inflow, the departure from the boundary-layer assumption $\partial P/\partial y = 0$ is small, and appears to be due to the upstream influence of the corner. In the corner and base region, the pressure field is strongly two-dimensional.

Part D is a contour plot of stagnation pressure, or Bernoulli sum[26] $P_T = P + \frac{1}{2}(u^2 + v^2)$. Burggraf[27] has suggested this quantity as an indicator of viscous effects.††

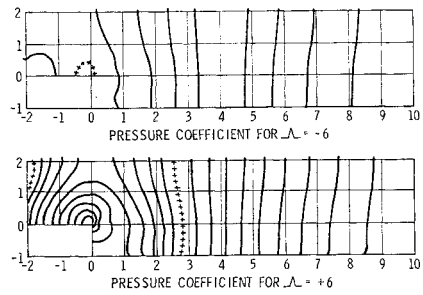

Fig. 3 Effect of inflow boundary-layer profile parameter Λ on the pressure distribution of incompressible backstep flow. R_0 = 100, δ/h = 1, no-slip centerline. For Λ = −6: ΔC_p = 0.02206 above +, ΔC_p = 0.00120 below +, C_p = 0 at +. For Λ = +6: ΔC_p = 0.01695 above +, ΔC_p = 0.01009 below +, C_p = 0 at +.

†† We have used $P_T = P + \frac{1}{2}(u^2 + v^2)$, following Burggraf[27] and Macagno and Hung.[26] A coefficient form, such as $C_{pT} = (P_T - P_0)/q_0$, would be preferable, since the numerical value of P_T depends on the level for P_0, arbitrarily set at $P_0 = 1$. However, contour lines of constant P_T are also contour lines of C_{pT}.

The gradient regions of P_T are seen to be confined to the viscous regions, with very little variation of P_T above the boundary layer and the free shear layer. In the boundary layer P_T generally follows the streamlines, as do other advection quantities. Some variation occurs along the splitter plate.

Figure 2 presents the effects of decreasing Reynolds number. Other conditions are the same as in Fig. 1, but with R_0 = 0.1. As indicated by the stream function plots, the separation point moves down from the sharp corner and reattachment moves forward toward the base as R_0 decreases. The DSL almost approaches a straight line. The standing vortex is much less vigorous, as indicated by the decrease in the magnitude of minimum ψ in the vortex, from 0.02948 at R_0 = 100, to 0.00096 at R_0 = 0.1, a ratio of 31–1. The growth of the boundary layer upstream of the corner is more pronounced.

As R_0 decreases the vorticity contour lines display less similarity to streamlines, indicating less dominance of advective transport.‡‡ Gradients near the sharp corner become less severe. Viscous effects extend above the inflow boundary-layer region. The pressure distribution departs considerably from the one-dimensional approximation, with appreciable y gradients existing at inflow and at outflow. At R_0 = 0.1, a positive C_p does not occur until 6 base heights downstream, and then only at the lid and centerline.

Examples of the vortex shedding at R_0 = 500 are given in Ref. 1.

The effect of varying the inflow boundary-layer profile, by varying Λ from −6 to +6, is surprisingly insubstantial, even at R_0 = 100. The only really pronounced effect is in the pressure solution, shown in Fig. 3. For Λ = −6, a negative C_p occurs only very close to the sharp corner. This is explained by an elementary one-dimensional description. The development of the Λ = −6 profile with a large velocity defect toward a profile with a smaller velocity defect resembles, one-dimensionally, the effect of a channel expansion, which tends to increase the pressure. The effect of Λ = +6 is the opposite; the negative pressure gradient ahead of the base being decreased algebraically.

Figure 4 presents the effect of removing the no-slip splitter plate. Other conditions are the same as in Fig. 1, including R_0 = 100 and δ/h = 1, but slip is allowed along the centerline, and symmetry gives $\xi_{\text{¢}}$ = 0. The main effect occurs at reattachment. It moves back to about $9\frac{1}{2}$ base heights downstream, compared to about $7\frac{1}{2}$ for a no-slip centerline, and the DSL near reattachment is now concave downward. Also, the standing vortex is more vigorous,

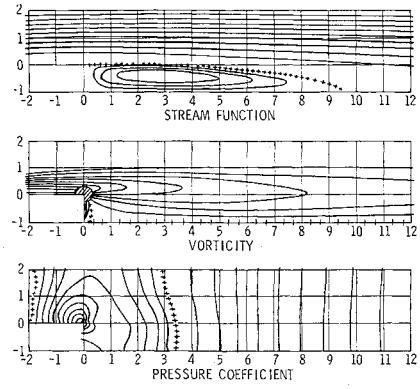

Fig. 4 Effect of slip C_L on incompressible flow over a backstep with R_0 = 100, δ/h = 1, Λ = 0, slip centerline. $\Delta\psi$ = 0.17000 above +, $\Delta\psi$ = 0.01284 below +, ψ = 0 at +. $\Delta\xi$ = 0.21637 above +, $\Delta\xi$ = 0.07954 below +, ξ = 0 at +. ΔC_p = 0.01966 above +, ΔC_p = 0.00601 below +, C_p = 0 at +.

‡‡ Also true of the plots of stagnation pressure and the source term of the Poisson equation for pressure.[1]

the magnitude of the minimum ψ having increased to 0.05136 from 0.02948, a ratio of 1.74:1. As a result, the gradients of vorticity and other transport properties near the corner are intensified. Since no boundary-layer redevelopment occurs along the slip centerline, the downstream pressure coefficient is now very close to being one-dimensional.

Some comparisons of the above effects are presented in Figs. 5–7. Within the limitations of the numerical method, we cannot truly isolate the separation and reattachment points; we can only infer their position by extrapolation of $\psi = 0$ to the walls. The movement of this extrapolated separation point down from the sharp corner as R_0 is decreased is presented in Fig. 5.

At $R_0 = 100$, the numerical solution indicates separation occurring at something less than one cell height ($h/10$) below the sharp corner. This viscous effect is somewhat exaggerated because of the implicit artificial viscosity effect of the upwind differencing. The location of separation will thus depend on the cell size, and can only be interpreted qualitatively at $R_0 = 100$. But, at $R_0 = 0.1$, the artificial viscosity effect is negligible. There are still not enough cells between the sharp corner and separation to accurately resolve this distance, especially since the corner geometry has deleterious effects on the accuracy.[1] But separation is indicated between 2 or 3 cells below the corner, so the phenomenon does not appear to be merely an aberration of the computational mesh.

Note also that separation is indicated below the sharp corner for all seven different methods of treating the sharp corner vorticity,[1] including one method intended to bias the solution toward separation at the corner, and two methods intended to *force* separation at the sharp corner.

Kawaguti[28] and Hung and Macagno[29] did not specifically mention separation from the base in their numerical studies of channel expansion. It is likely that they ignored indicated separation less than one cell below the corner and faired in the DSL to the assumed corner separation. Kawaguti[28] shows a small dotted-line segment below the indicated DSL near the corner, with no comment; this is probably the actual computed DSL.

The effect of Λ and a slip centerline on the separation distance are confined to less than $\frac{1}{2}$ cell, and therefore cannot be accurately compared. But the effects on reattachment distance are shown in Fig. 5. The effect of Λ is small.

When plotted on a linear R_0 scale, the separation distance does not show the linear variation with R_0 as found by Kawaguti[28] and by Hung and Macagno[29] in channel expansions. The present case differs from these in several respects, notably in the boundary conditions used. The present nonlinear trend is probably due to the influence of the upper wall. But another significant point is that these authors do not show the DSL concave upwards at reattachment, and do not indicate precisely how the reattachment point was located. In the present study, reattachment was located in the computer program itself by linear extrapolation of $\psi = 0$ from the first and second node points above the centerline. With the DSL concave outward, this gave reattachment further downstream than would be obtained by extrapolating the last few $\psi = 0$ points to a symmetry condition $(\partial\psi/\partial y)_{\psi=0} = 0$, as apparently done by Kawaguti.

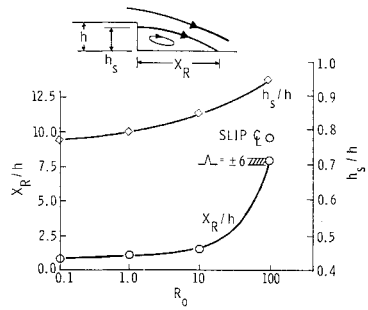

Fig. 5 Extrapolated separation and reattachment distances for incompressible flow over a backstep. Basic case: $R_0 = 100$, $\Lambda = 0$, $\delta/h = 1$, no-slip centerline.

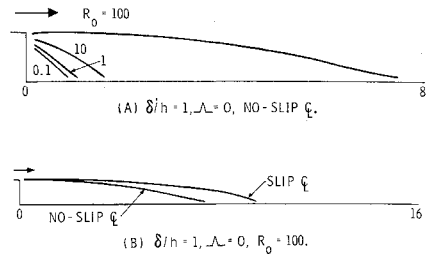

Fig. 6 Comparison of dividing streamlines for incompressible flow over backsteps.

The arbitrariness of linear extrapolation is best avoided by comparing the DSL of various situations without any extensions to the walls. This is done in Fig. 6. This figure especially clarifies the effect of the no-slip centerline in moving the DSL downstream. This effect was actually minimized at reattachment due to the difference in concavity of the DSL. The other effects also show up more clearly.

The effects of the various parameters on the average§§ base pressure coefficient C_{pB} and the pressure coefficient at reattachment C_{pR} are shown in Fig. 7. These both show a strong dependence on R_0, especially C_{pB}, in the range of R_0 from 0.1 to 100, but the effect is starting to level off at 100, as expected. There is little effect of Λ, as before. It is surprising that, although a slip centerline causes a more vigorous vortex and a longer DSL, the C_{pB} and C_{pR} are affected very little. The only important contributor to C_{pB} seems to be R_0. This fact may be of importance to flow model theories.

The effect of base bleed is easily modeled numerically in incompressible flow. An example can be found in Ref. 1.

Also in Ref. 1 are the contour plots of temperature for the same flow conditions as Fig. 1, with uniformly cold inflow and a uniformly hot base and splitter plate. The average and local base Nusselt numbers for this flow are plotted in Fig. 8. The Nusselt number is highest near the corner because of the change in boundary temperature there, and of course it is zero at the base/splitter plate intersection. The average base Nusselt number $\hat{N}u_B$ decreases with increasing Eckert number E in an accurately linear manner. The slopes between $E = 0.0$–0.1, and between $E = 0.0$–1.0, differed less than 0.1%, which difference is possibly due to machine round-off error.

Figure 9 presents contour plots of stream function and vorticity for forced flow over a square cavity at $R_0 = 100$. The mesh configuration consisted of a 10×10 cell cavity in a 30×30 cell field, with $\beta = \Delta x/\Delta y = 1$. At the inflow, located one cavity depth upstream, a Pohlhausen boundary-layer profile was again used, with $\delta/h = 1$ and $\Lambda = 0$. Both separation and reattachment occur below the sharp corners, and the DSL is concave downwards. Very little effect is seen on the stream function above the cavity, but a slight

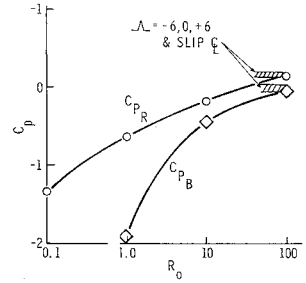

Fig. 7 Average base pressure coefficient and pressure coefficient at reattachment for incompressible flow over a backstep. Basic case: $R_0 = 100$, $\Lambda = 0$, $\delta/h = 1$, no-slip centerline.

§§ The average does not include the extreme mesh points of the base.

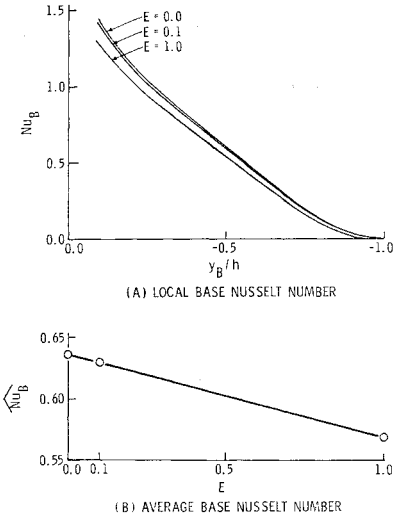

Fig. 8 Effect of Eckert number on local and average base Nusselt number for incompressible flow over a backstep. $R_0 = 100$, $\delta/h = 1$, $\Lambda = 0$, no-slip centerline. $T_B = 1$, T centerline $= 1$, inflow boundary layer $T(y) = 0$, $Pr = 1$. For stream function, etc., see Fig. 1.

downward movement of the first streamline is discernible.¶¶ The vortex center is very slightly downstream of the cavity center and about $\frac{1}{4}$ of the cavity depth above the cavity center. The vorticity contours show the expected high gradients near both corners, and a decrease in gradient above the cavity opening.

For the $R_0 = 1000$ case,[1] completely steady flow exists, whereas the same conditions for a backstep caused vortex shedding at much lower R_0. The stream function in the external stream is even less affected than for $R_0 = 100$. The vortex center is shifted in the downstream direction.

The present cavity flow solutions differ from those of Kawaguti,[30] Burggraf,[27] and Pan and Acrivos[31] in the high R_0 attained, but most importantly in that forced flow over the cavity was specified. These authors considered a driven cavity with constant $u = 1$ along the top of the cavity, thus modeling a moving wall with the DSL fixed at the lid of the cavity. The resulting shear is much higher and the vortex more vigorous, all other conditions being equal. Thus, Burggraf[27] shows a secondary vortex existing below $R_0 = 400$ (his limit of computational stability), whereas the present results show none even at $R_0 = 1000$. But obviously the numerical solution cannot reveal motions at a scale smaller than the mesh size, so it is possible that such small-scale recirculation regions would exist physically.

VI. Numerical Results for Compressible Flow

For the compressible flow equations, the critical time step from Kurzrock's analysis[8] is impractically limiting for the present cases where recirculation regions exist, which necessitated the use of a very coarse computing mesh, with only 5 cells along the base. Consequently, the results are not accurate; we draw conclusions only from the gross qualitative behavior of the calculations.

A backstep geometry similar to that shown in Fig. 1 was used, with $\delta/h = 1$,* $\gamma = 1.4$, and $Pr_0 = 1$. The inflow boundary conditions are those of the adiabatic wall boundary-layer solution for zero pressure gradient given by Cohen and Reshotko.[32]

As in incompressible flow, the DSL is concave downwards near reattachment to a slip centerline, and concave upwards at reattachment to a no-slip centerline. The average base pressure decreases as R_0 decreases and M_0 increases. Compressibility greatly shortens the distance to reattachment. For a calculation at $M_0 = u_0/c_0 = 2.236$ and $R_0 = 300$ with μ constant, reattachment was indicated between 3 and 4 base heights downstream; an incompressible solution at the same R_0 and in the same crude mesh indicated a reattachment distance of 23 base heights.

Separation was always indicated below the sharp corner, and moved down as R_0 was decreased or M_0 increased. As in incompressible flow, this viscous effect is exaggerated because of the implicit artificial viscosity effect of the upwind differencing, but there can be little doubt that the phenomenon exists. Other solutions[1] obtained with another mesh system, in which a node point is located on the sharp corner, also show separation off the base, indicating that the phenomenon is not a quirk of the boundary treatment.

The effect of including variable viscosity, with $\mu \propto T$, was very strong. At $M_0 = 2.236$, the flowfield encompasses greater than a fourfold variation in temperature, and hence in μ. This greatly increases the shear stress in the separated flow region. For $R_0 = 300$, the average base pressure is reduced about 10%, the reattachment distance decreases to about one base height, and the separation point moves further down from the sharp corner.

The sensitivity to variable μ would be decreased by the use of a more realistic viscosity-temperature relation, but the indication of these results is that the variability of flow properties has important effects on the total solution.

VII. A Discussion of Viscous Separation in the Vicinity of a Sharp Corner

The present numerical results are especially interesting in that, for all cases, for both incompressible and supersonic flows, for steady and nonsteady backstep flows and cavity flows, and for several different treatments of the sharp corner boundary conditions and finite difference mesh configurations, the extrapolated separation point occurs below the sharp corner. This is in agreement with Hama,[33,34] who was the first to claim, on the basis of experimental observations, that separation does not occur at the sharp corner of a backstep-type laminar supersonic flow, but occurs below the corner, off the base. He also demonstrated the connection of this phenomenon with the lip shock. Donaldson[35] has presented substantiating experimental evidence. Weinbaum[36] developed an incompressible theory, based on a Stokes linearization, which also predicts the phenomenon of separation below the sharp corner, albeit dependent upon two undetermined coefficients. Browand[37] has observed the dye-marked DSL to separate almost halfway down the base of a wedge in glycerine tank experiments. Allen[25] has also obtained this result in finite difference calculations of the supersonic near wake problem, in a much finer mesh than used in the present calculations.

Our present incompressible numerical results show a regular movement of the separation point down the base as R_0 is decreased. This tendency is in agreement with the well-known incompressible result at $R_0 = 0$ for Stokes flow over a sphere, in which no separation occurs, and with Underwood's[38] recent

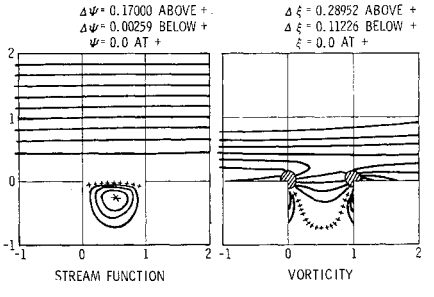

Fig. 9 Incompressible forced flow over a square cavity. $R_0 = 100$, $\delta/h = 1$, $\Lambda = 0$.

¶¶ This is verified by complete digital results.

* δ based on $u = 0.98u_e$.

solution for the incompressible flow over a circular cylinder obtained by the semianalytic method of series truncation. He finds no separation below a Reynolds number (based on cylinder diameter) of 5.75. However, the numerical results of Hung and Macagno[29] show a separation region at $R_0 = 0$ in a channel expansion, approximately with the same streamline pattern as the results at $R_0 = 0.1$. Also, Burggraf[27] presents a driven cavity numerical solution at zero Reynolds number which displays a secondary eddy, indicating again that separation is possible. Thus it appears from the present results that the Stokes flow limit does give separation below the sharp corner, but that for the backstep geometry, $R_0 = 0$ does not necessarily imply a flow configuration devoid of separation, as the present authors had originally assumed.[1]

Our supersonic flow solutions show the same movement of separation down the base, more than one cell below the corner, both for cases of constant properties and for cases of temperature-variable properties. The effect of variable properties is to accentuate the downward movement of the separation point. An $R_0 = 0$ limit position of separation below the sharp corner also appears to be indicated for the compressible flow equations, although the equations are then no longer valid, since the continuum assumption fails.

The phenomenon of viscous separation below the corner, first found experimentally by Hama[33,34] in supersonic flow, is then simply interpretable, in both supersonic and in incompressible flows, as a movement of the separation point down from the (conjectured) limit position at the sharp corner toward a Stokes flow limit as R_0 is decreased.

VIII. Summary

Numerical techniques and solutions for both incompressible and compressible laminar separated flows using time-dependent finite difference equations have been presented. These included backstep or base flows, with and without splitter plates, and flow over square cavities. Conservative forms were used, and upwind differencing was used for the advection terms in both compressible and incompressible flow. The Transportive Property was defined. This property of the differencing scheme maintains the integral kinematic properties of the continuum solution, in the same way that the well-known Conservative Property maintains the integral Gauss Divergence Theorem properties of the continuum solution.

A method due to Miyakoda was used to obtain nondrifting solutions of the Poisson form of the incompressible pressure equation with von Neumann boundary conditions. A two-time level predictor-corrector analogue of the Du Fort-Frankel scheme was used for diffusive terms in the compressible flow to achieve computational stability at low Reynolds numbers. Particular attention was given to the boundary-condition problems, especially the vorticity at the sharp corner, the developing inflow, and the downstream continuation in incompressible flow, and the adjusting inflow through the top of the mesh and the wall density in supersonic flow. Computational stability was maintained throughout the range of parameters investigated; for incompressible flow, the step height R_0 ranged from 10^{-1} to 10^5; and, for the compressible flow, the Reynolds number ranged from 10 to 10^5, and the Mach numbers up to 6.

The major numerical results were as follows. For the backstep and cavity geometries, contour plots of pressure, vorticity, and streamlines were presented. The dividing streamline appears concave upwards near recompression at a no-slip surface, but concave downwards at a slip surface. For the case of incompressible, uniformly cold flow over a backstep with a hot base and hot splitter plate, the base heat transfer was seen to vary linearly with Eckert number. The effect of variable viscosity was shown to strongly affect the supersonic near-wake solution, moving the separation point further down from the corner and the reattachment point closer to the base.

Finally, the phenomenon of backstep separation off the base below the sharp corner, which was first found experimentally by Hama in supersonic flow, was demonstrated in both incompressible and compressible flow. The separation point moves down from the conjectured limit position at the sharp corner toward a Stokes flow limit as the Reynolds number is decreased.

References

[1] Roache, P. J., *Numerical Solutions of Compressible and Incompressible Laminar Separated Flows*, Ph.D. dissertation, Dept. of Aero-Space Engineering, Univ. of Notre Dame, Notre Dame, Ind., Nov. 1967; also Roache, P. J. and Mueller, T. J., AIAA Paper 68-741, Los Angeles, 1968.

[2] Lax, P. D., "Weak Solutions of Nonlinear Hyperbolic Equations and Their Numerical Computations," *Communications in Pure and Applied Mathematics*, Vol. 7, 1954, pp. 159–193.

[3] Lilly, D. K., "On the Computational Stability of Numerical Solutions of Time-Dependent Non-Linear Geophysical Fluid Dynamics Problems," *U.S. Weather Bureau Monthly Weather Review*, Vol. 93, No. 1, Jan. 1965, pp. 11–26.

[4] Forsythe, G. E. and Wasow, W., *Finite Difference Methods for Partial Differential Equations*, Wiley, New York, 1960, pp. 444.

[5] Frankel, S. P., "Some Qualitative Comments on Stability Considerations in Partial Difference Equations," *Proceedings of the Sixth Symposia in Applied Mathematics*, American Mathematical Society, Vol. VI, 1956, McGraw-Hill, New York, pp. 73–75.

[6] Motzkin, T. S. and Wasow, W., "On the Approximation of Linear Elliptic Differential Equations by Difference Equations with Positive Coefficients," *Journal of Mathematics and Physics*, Vol. 31, 1953, pp. 253–259.

[7] Roberts, K. V. and Weiss, N. O., "Convective Difference Schemes," Nov. 1964, United Kingdom Atomic Energy Authority, Culham-Laboratory, Abingdon, Berks, England; also *Mathematics of Computation*, Vol. XX, No. 94, April 1966.

[8] Kurzrock, J. W., *Exact Numerical Solutions of the Time-Dependent Compressible Navier-Stokes Equations*, Ph.D. dissertation, Cornell Univ., CAL Rept. AG-2026-W-1, Feb. 1966; also Kurzrock, J. W. and Mates, R. E., AIAA Paper 66-30, New York, 1966.

[9] Richtmeyer, R. D., *Difference Methods for Initial-Value Problems*, Interscience, New York, 1957, p. 238.

[10] Stone, H. L. and Brian, P. L. T., "Numerical Solution of Convective Transport Problems," *AIChE. Journal*, Vol. 19, 1963, pp. 681–688.

[11] Richtmeyer, R. D., "A Survey of Difference Methods for Nonsteady Fluid Dynamics," NCAR TN 63-2, 1963, National Center for Atmospheric Research, Boulder,Colo.

[12] Courant, R., Isaacson, E., and Rees, M., "On the Solution of Nonlinear Hyperbolic Differential Equations by Finite Differences," *Communications in Pure and Applied Mathematics*, Vol. 5, No. 243, 1952.

[13] Longley, H. J., "Methods of Differencing in Eulerian Hydrodynamics," Rept. LAMS-2379, 1960, Los Alamos Scientific Lab., Los Alamos, N. Mex.

[14] Filler, L. and Ludloff, H. F., "Stability Analysis and Integration of the Viscous Equations of Motion," *Mathematics of Computation*, Vol. 15, July 1961, pp. 261–274.

[15] Gentry, R. A., Martin, R. E., and Daley, B. J., "An Eulerian Differencing Method for Unsteady Compressible Flow Problems," *Journal of Computational Physics*, Vol. 7, 1966, pp. 87–118.

[16] Thoman, D. C. and Szewczyk, A. A., "Numerical Solutions of Time Dependent Two Dimensional Flow of a Viscous, Incompressible Fluid Over Stationary and Rotating Cylinders," TR 66-14, July 1966, Heat Transfer and Fluid Mechanics Lab., Univ. of Notre Dame; to be published in *The Physics of Fluids Supplement*.

[17] Schlichting, H., *Boundary Layer Theory*, 4th ed., McGraw-Hill, New York, 1960, p. 647.

[18] Fromm, J., "A Method for Computing Nonsteady Incompressible Viscous Fluid Flows," Rept. LA-2910, 1963, Los Alamos Scientific Lab., Los Alamos, N. Mex.

[19] Harlow, F. H. and Fromm, J. E., "Dynamics and Heat Transfer in the von Kármán Wake of a Rectangular Cylinder," *The Physics of Fluids*, Vol. 7, No. 8, Aug. 1964, pp. 1147–1156.

[20] Jenson, V. G., "Viscous Flow Round a Sphere at Low Reynolds Numbers ($\leq$40)," *Proceedings of the Royal Society, Series A*, Vol. 249, 1959, pp. 346–366.

[21] Miyakoda, K., "Contribution to the Numerical Weather Prediction—Computation with Finite Difference," *Japanese Journal of Geophysics*, Vol. 3, 1962, pp. 75–190.

[22] Courant, R., Friedrichs, K. O., and Lewy, H., "Über die Partiellen Differenzengleichurgen der Mathematischen Physik," *Matematische Annalen*, Vol. 100, 1928, pp. 32–74.

[23] Du Fort, E. C. and Frankel, S. P., "Stability Conditions in the Numerical Treatment of Parabolic Differential Equations," *Mathematical Tables and Other Aids to Computation*, Vol. 7, 1953, pp. 135–152.

[24] Eaton, R. R. and Zumwalt, G. W., "A Numerical Solution for the Flow Field of a Supersonic Cone-Cylinder Entering and Leaving a Blast Sphere Diametrically," SC-CR-67-2532, May 1967, Sandia Lab., Albuquerque, N. Mex.

[25] Allen, J. S., "Numerical Solutions of the Compressible Navier-Stokes Equations for the Laminar Near Wake in Supersonic Flow," Ph.D. dissertation, Princeton Univ., June 1968; also Allen, J. S. and Cheng, S. I., *AGARD Specialists Meeting in Numerical Methods for Fluid Mechanics*, Sept. 1967.

[26] Macagno, E. O. and Hung, T. K., "Pressure, Bernoulli Sum, and Momentum and Energy Relations in a Laminar Zone of Separation," *The Physics of Fluids*, Vol. 10, No. 1, Jan. 1967, pp. 78–82.

[27] Burggraf, O. R., "Analytical and Numerical Studies of the Structure of Steady Separated Flows," *Journal of Fluid Mechanics*, Vol. 24, Pt. 1, 1966, pp. 113–152.

[28] Kawaguti, M., "Numerical Solutions of the Navier-Stokes Equations for the Flow in a Channel with a Step," Tech. Summary Rept. 574, 1965, Mathematics Research Center, Univ. of Wisconsin, Madison, Wis.

[29] Hung, W. T.-K. and Macagno, E. O., "Laminar Eddies in a Two-Dimensional Conduit Expansion," *La Houille Blanche*, Vol. 21, No. 4, 1966, pp. 391–400.

[30] Kawaguti, M., "Numerical Solution of the Navier-Stokes Equations for the Flow in a Two-Dimensional Cavity," *Journal of the Physical Society of Japan*, Vol. 16, Nov. 1961, pp. 2307–2315.

[31] Pan, F. and Acrivos, A., "Steady Flows in Rectangular Cavities," *Journal of Fluid Mechanics*, Pt. 4, 1967, pp. 643–655.

[32] Cohen, C. B. and Reshotko, E., "Similar Solutions for the Compressible Laminar Boundary Layer with Heat Transfer and Pressure Gradient," TR 1293, 1956, NACA.

[33] Hama, F. R., "Experimental Investigations of the Base Flow Problem. II. Wedge," *Space Programs Summary 37-37*, Vol. IV, Oct. 1965, Jet Propulsion Lab., Pasadena, Calif., pp. 237–240.

[34] Hama, F. R., "Experimental Studies on the Lip Shock," *AIAA Journal*, Vol. 6, No. 2, Feb. 1968, pp. 212–219.

[35] Donaldson, I. S., "On the Separation of a Supersonic Flow at a Sharp Corner," *AIAA Journal*, Vol. 5, No. 6, June 1967, pp. 1086–1088.

[36] Weinbaum, S., "On the Singular Points in the Laminar Two-Dimensional Near Wake Flowfield," *Journal of Fluid Mechanics*, Vol. 33, Pt. 1, 1968, pp. 38–63.

[37] Browand, F. K., private communication, Univ. of Southern Calif., Jan. 1968.

[38] Underwood, R. L., "Calculation of Incompressible Flow Past a Circular Cylinder at Moderate Reynolds Numbers," *Journal of Fluid Mechanics*, Vol. 37, Pt. 1, 1969, pp. 95–114.